AIP | Review of Scientific Instruments

Four degree of freedom liquid dispenser for direct write capillary self-assembly with sub-nanoliter precision

Justin Beroz, Mostafa Bedewy, Michael Reinker, Vipul Chhajer, Shorya Awtar et al.

Citation: Rev. Sci. Instrum. **83**, 015104 (2012); doi: 10.1063/1.3673680
View online: http://dx.doi.org/10.1063/1.3673680
View Table of Contents: http://rsi.aip.org/resource/1/RSINAK/v83/i1
Published by the American Institute of Physics.

Four degree of freedom liquid dispenser for direct write capillary self-assembly with sub-nanoliter precision

Justin Beroz, Mostafa Bedewy, Michael Reinker, Vipul Chhajer, Shorya Awtar, and A. John Hart[a)]
Department of Mechanical Engineering, University of Michigan, Ann Arbor, Michigan 48109, USA

(Received 2 November 2011; accepted 6 December 2011; published online 9 January 2012)

Capillary forces provide a ubiquitous means of organizing micro- and nanoscale structures on substrates. In order to investigate the mechanism of capillary self-assembly and to fabricate complex ordered structures, precise control of the meniscus shape is needed. We present a precision instrument that enables deposition of liquid droplets spanning from 2 nl to 300 μl, in concert with mechanical manipulation of the liquid-substrate interface with four degrees of freedom. The substrate has sub-100 nm positioning resolution in three axes of translation, and its temperature is controlled using thermoelectric modules. The capillary tip can rotate about the vertical axis while simultaneously dispensing liquid onto the substrate. Liquid is displaced using a custom bidirectional diaphragm pump, in which an elastic membrane is hydraulically actuated by a stainless steel syringe. The syringe is driven by a piezoelectric actuator, enabling nanoliter volume and rate control. A quantitative model of the liquid dispenser is verified experimentally, and suggests that compressibility in the hydraulic line deamplifies the syringe stroke, enabling sub-nanoliter resolution control of liquid displacement at the capillary tip. We use this system to contact-print water and oil droplets by mechanical manipulation of a liquid bridge between the capillary and the substrate. Finally, we study the effect of droplet volume and substrate temperature on the evaporative self-assembly of monodisperse polymer microspheres from sessile droplets, and demonstrate the formation of 3D chiral assemblies of micro-rods by rotation of the capillary tip during evaporative assembly. © *2012 American Institute of Physics*. [doi:10.1063/1.3673680]

I. INTRODUCTION

Central to the creation of new materials is the study of how geometric arrangements of constituent building blocks can determine macroscale material properties. In particular, the size, spacing, and arrangement of micro- and nanoparticles can determine the optical, electric, and thermal characteristics of a surface or bulk crystal. Applications of particle assemblies include optoelectronics,[1] photonics,[2] biological sensors,[3] granular electronics,[4] lithography,[5] and spectroscopy.[6] However, in order to realize these applications, as well as enable fundamental studies of different crystalline arrangements, simple and scalable techniques are needed to assemble nanoparticle structures with deterministic shape and crystalline order.

When particles are suspended in a liquid, the proportional relationship between meniscus curvature and capillary pressure drives particles to assemble in ordered arrangements at the liquid-air interface.[7] This phenomenon, typically called evaporative self-assembly, has been exploited to assemble closely packed clusters and monolayers of micro- and nanoparticles.[8] Additionally, it has been shown that the shape of the meniscus during evaporation can influence the geometry and crystal structure of particle assemblies.[9] For example, discrete clusters of microparticles have been made by simply drop-casting microliter volumes of solution onto a substrate with lithographically patterned wells.[10] Similarly, micro molds have been used to confine the meniscus into various two-dimensional (2D) shapes, including squares, hexagons, and circular rings,[11] resulting in matching particle arrangements.

Several direct-write methods have been used to controllably deposit small volumes of liquid onto substrates. These are typically engineered for printing droplets onto unpatterned substrates, where evaporation occurs without additional mechanical constraint. These include noncontact systems that print onto substrates by pressure-driven,[12] electrohydrodynamic,[13] and pyroelectrodynamic[14] droplet ejection. Additionally, there are contact printing methods that include dip-pen printing with micro quills or AFM tips,[15] inkjet nozzle dispensing driven by a stepper motor,[16] and ultrasonic pumping through a capillary pipette tip.[17] Direct-write methods have also been used to print complex three-dimensional (3D) polymer and ceramic lattice structures,[18] spanning microelectrodes,[19] and 3D polycrystalline colloid structures by multi-layer deposition.[20]

We propose that dynamic manipulation of the meniscus during assembly could enable fabrication of more complex 2D and 3D particle assemblies and, further the mechanistic understanding of capillary-force-driven evaporative self-assembly of micro- and nanoparticle crystals. Such a technique would combine the functionality of direct-write approaches that dispense precise liquid volumes onto substrates, and templating approaches that physically direct the meniscus during evaporation.

Therefore, we present a system for direct-write capillary self-assembly which enables simultaneous controlled

a)Electronic mail: ajohnh@umich.edu.

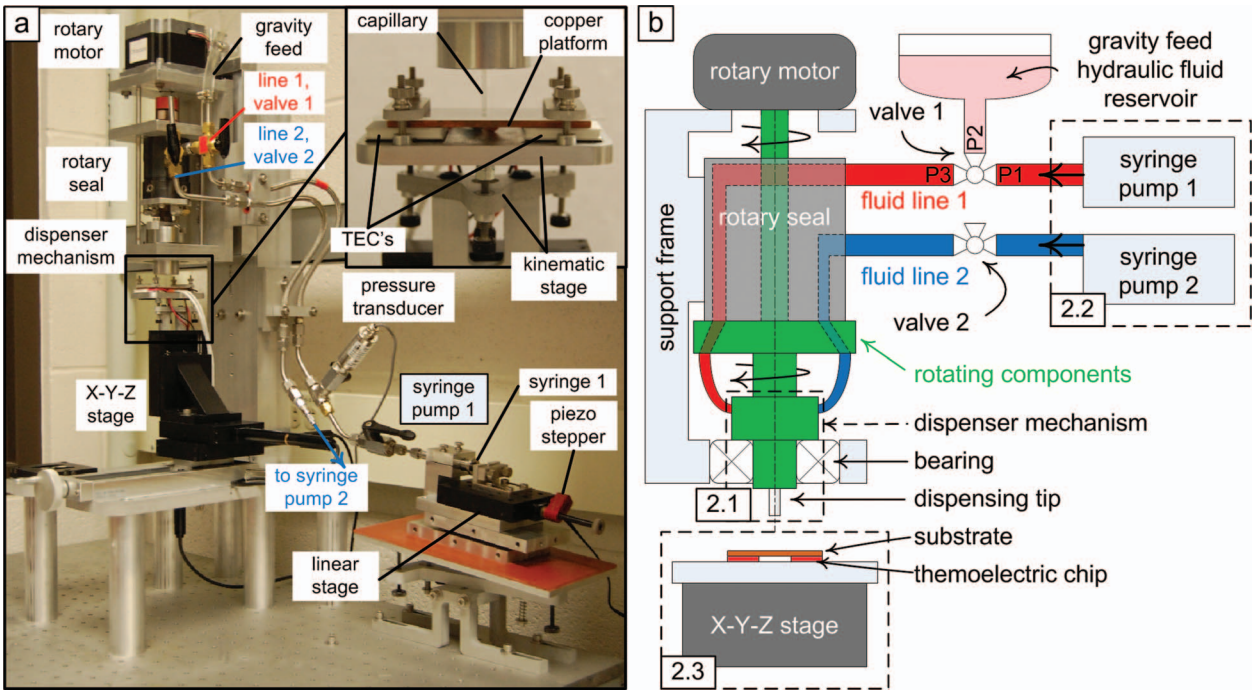

FIG. 1. (Color online) Instrument for direct-write meniscus manipulation: (a) complete assembly on optical tabletop; (b) schematic representation showing fluid and motion paths in the system.

deposition and manipulation of liquid droplets in four degrees of freedom. This system features a novel diaphragm pumping mechanism that has bidirectional control of liquid volumetric displacement and rate, with sub-nanoliter accuracy. This is enabled by a custom-built syringe pump controlled by a piezo-stepper motor. The system can deposit liquid volumes spanning from 2 nl to 300 μl, due to its variable volume loading capability. This liquid may be diluted, mixed, or stratified by a secondary fluid. Additionally, the substrate may be controllably heated and cooled to influence the liquid evaporation rate. We demonstrate the use of this system in two exemplary experiments: (1) combinatorial screening of how droplet size and substrate temperature affect the crystallization of 2D islands of polymer microparticles from suspension and (2) building a 3D chiral assembly of polymer microcylinders by rotation of the capillary tip during liquid dispensing and evaporation.

II. SYSTEM DESIGN AND CONSTRUCTION

The direct-write liquid manipulation system (Fig. 1) can simultaneously dispense liquid and control the motion between a dispensing (capillary) tip and a temperature-controlled substrate. The system comprises a dispenser mechanism, translation stage assembly, rotary seal and motor, two fluid lines, and two syringe pumps. The substrate translates in three axes (X-Y-Z) and the tip rotates about the vertical axis (θ) perpendicular to the substrate. The syringe pumps control the volumetric displacement of the fluid in their respective stainless steel lines. Syringe pump 1 is custom built and syringe pump 2 is a commercial product (New Era Pump Systems Inc., NE-510). Valves 1 and 2 are used for line filling and pressure relief.

Both fluid lines pass through the rotary seal (Rotary Systems Inc., 003-10210) and feed into the dispenser mechanism. Actuation of the syringe pump(s) is transmitted hydraulically through the fluid lines to control displacement of a "deposition fluid" through the capillary tip, which is separated from the hydraulic fluid by an elastic diaphragm. The rotary seal contains an inner component that turns with respect to an outer stationary casing, allowing the fluid line input and output ports to rotate with respect to one another. The rotary motor turns the inner rotary seal component. The rotary motor, rotary seal, and dispenser mechanism are connected about a single axis of rotation so that the rotary motor turns the entire dispenser mechanism, which is seated in a sealed ball bearing (McMaster, 2780T68). As discussed later, the stiffness of the diaphragm and the compressibility (due to trapped air) of the hydraulic fluid present a straightforward means to achieve high-resolution control of liquid displacement in the capillary.

A. Dispenser mechanism and diaphragm pump

The dispenser mechanism enables liquids to be loaded into a reservoir and controllably dispensed through a capillary tip. It consists of the following components (Figs. 2(a) and 2(b)):

1. A reservoir for the deposition liquid, which is formed by the elastic diaphragm and stainless steel contoured bowl.
2. A clamping block that holds the diaphragm against the flat perimeter of the contoured bowl, and connects to the hydraulic line.
3. An inlet port, which is opened to load deposition liquid and plugged during dispensing.

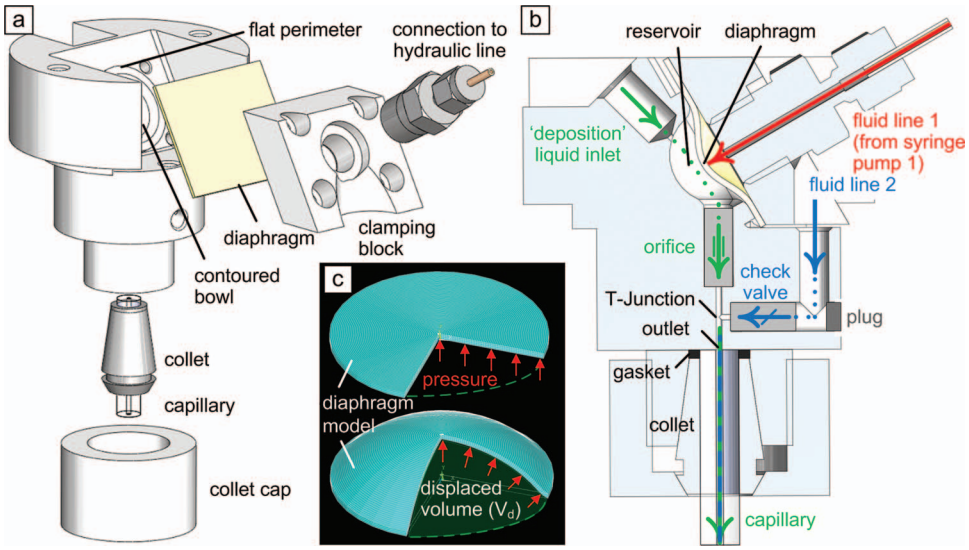

FIG. 2. (Color online) Model and schematic of dispenser mechanism: (a) exploded view, showing how diaphragm is clamped over the bowl and capillary is held using a collet; (b) cross-section indicating flow paths; (c) finite element model of elastic diaphragm deformation.

4. A T-junction for fluid mixing using the second line.
5. An assembly of a miniature collet and collet cap, which holds the capillary tube along the axis of rotation, and can accommodate capillary tips with different diameters.

The elastic diaphragm, fluid line 1, and syringe pump 1 comprise a hydraulic pump which is used to control the displacement of the deposition liquid through a capillary tip. The elastic diaphragm is hydraulically actuated by volumetric displacement of the fluid in line 1 using the syringe pump 1 (Fig. 1(a)) which is described in Sec. II B.

The contour of the reservoir bowl is designed to approximately match the deformed shape of the elastic diaphragm under applied hydraulic pressure. This was verified by simulating the deformed diaphragm contour using nonlinear finite element analysis in ANSYS (Fig. 2(c)). We use a square Latex sheet (McMaster, 8611K222) for the diaphragm, although any stretchable material flexible enough to conform to the surface of the reservoir bowl would be suitable. Cutting from a sheet is cost-effective and allows the diaphragm material to be selected based on its mechanical properties and chemical compatibility with the contacting fluids.

The reservoir is loaded by first actuating the diaphragm forward (via fluid line 1) until it conforms to the bowl surface. Next, a micropipette tip filled with the deposition liquid is placed in the inlet port. The diaphragm is then actuated away from the bowl surface, drawing the liquid into the reservoir from the pipette. The pipette is then removed and replaced with a stopper to plug the inlet hole. The reservoir volume may be adjusted from ~0 to 300 μl based on how far the diaphragm is drawn backward during the liquid loading step. Liquid is dispensed from the reservoir by actuating the diaphragm forward, which displaces the liquid through the orifice and capillary tube.

A miniature collet holds the capillary tube and centers it about the axis of rotation. A screw cap holds the collet against the capillary and squeezes the top end of the capillary against a gasket to maintain the internal seal. A secondary fluid in line 2 can be fed into the capillary via a T-junction beneath the reservoir bowl by positive displacement of syringe pump 2. This secondary fluid may be used to dilute or mix with the deposition liquid.

B. Syringe pump

We initially used a commercially available syringe pump to actuate the diaphragm, but the step resolution (~5 μm) and backlash (~300 μm) of its lead screw mechanism were insufficient for our needs. In particular, the backlash prevented consistent reversible control of fluid dispensing, which we later show to be essential for dispensing nanoliter droplets by contact printing.

As a result, we constructed a custom syringe pump consisting of a stainless steel syringe (New Era Pump Systems Inc., SYR-SS1SL8) actuated linearly on a micrometer stage (Thorlabs, PT1) by a piezo-stepper motor (New Focus, 8303). This motor drives the volume and rate of fluid displacement of the syringe with <30 nm step size and <15 nm backlash, and is controlled through LabVIEW.

C. Stage assembly

The stage assembly holds the substrate, which is typically a piece of silicon wafer or a glass slide. The stage is a copper platform suspended between two thermoelectric chips (Custom Thermoelectric, 12711-5L31-02CK), as illustrated in Fig. 1(a). The thermoelectric chips are driven in parallel by a single temperature controller (Omega, CNi3242-C24), with feedback from a thermocouple mounted underneath the platform. The suspended platform design provides spatial uniformity of temperature in the center of the suspended region.[21] With this setup, we can control the substrate temperature from 20–70 °C, and have measured heating rates as rapid as 1.4 °C/sec.

The stage assembly is supported by a custom-made 3-point ball-groove kinematic coupling (Fig. 1(a)), which

enables fine adjustment of the substrate's planar orientation. This entire assembly is fixed to three linear actuated stages, arranged serially, which enable three-dimensional positioning. Each actuator (Thorlabs, Z825B) has 28 nm incremental resolution and is controlled using the LabVIEW.

III. LIQUID DISPENSER MODEL AND CHARACTERIZATION

The custom syringe pump (syringe pump 1) displaces the fluid in line 1, which deforms the elastic diaphragm inside the dispenser. In this section, we describe how the design parameters of this hydraulic diaphragm pump (Fig. 3(a)) determine the volume of liquid dispensed from the reservoir (∂V_d, [m^3]) upon syringe actuation (∂V_s, [m^3]). This model was motivated by our practical finding that entrapment of a small amount of air is inevitable when filling the hydraulic line, largely due to the intricate geometry inside the rotary seal component. Therefore, ∂V_s is not exactly equal to ∂V_d, as would be the case if the hydraulic line was incompressible. Notably, the inclusion of this entrapped air deamplifies ∂V_d with respect to ∂V_s, which significantly increases the system's resolution.

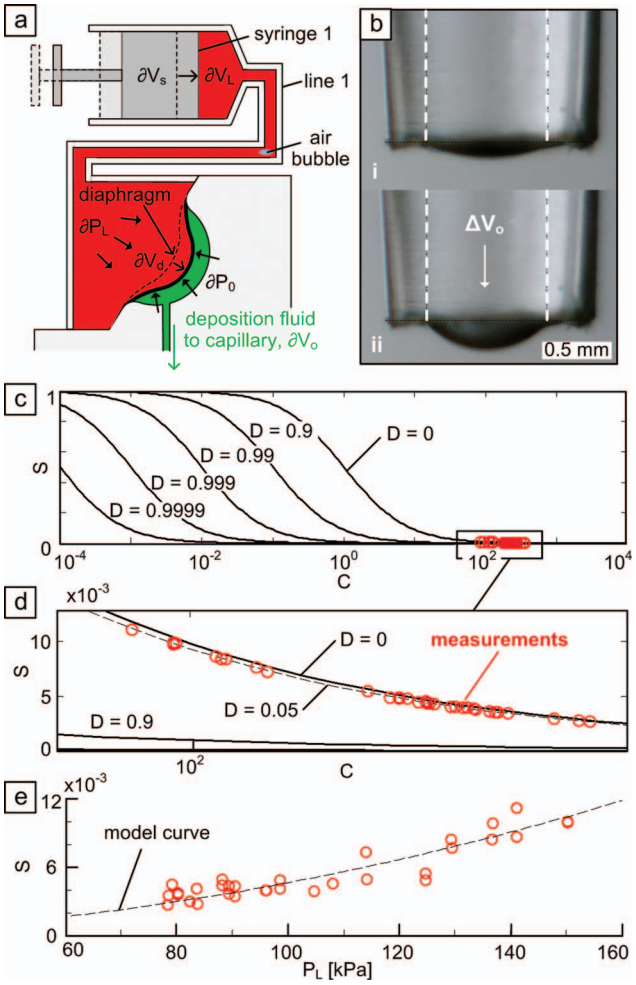

FIG. 3. (Color online) (a) Schematic of components and parameters comprising the diaphragm pump that contribute to the system model; (b) representative liquid displacement at the capillary tip for sensitivity measurements; (c) system model depicts that the nonlinear curve relating sensitivity (S) and line compressibility (C) shifts left as disturbance (D) increases; (d) experimental sensitivity measurements (circles) fall within a fixed C range and along model curve for $D = 0.05$; (e) the system model accurately describes the explicit experimental relation between sensitivity measurements at various line pressures.

We determined several physical relations among the system parameters defined in Fig. 3(a). First, the volume of air (V_{air}, [m^3]) and volume of hydraulic fluid (V_f, [m^3]) constitute the total volume of the hydraulic line (V_L, [m^3]) (Eq. (1)),

$$V_L = V_f + V_{\text{air}}. \tag{1}$$

Compressibility in the hydraulic line may be attributable to entrapped air (n, [mol]) as described by the ideal gas law (Eq. (2)), and to hydraulic fluid compression (β, [Pa^{-1}]) (Eq. (3)). R is the universal gas constant and T is the absolute room temperature. It is assumed that the stainless steel tubing that houses the hydraulic fluid is rigid,

$$P_L V_{\text{air}} = nRT, \tag{2}$$

$$\frac{\partial V_L}{\partial P_L} = -\left(\frac{nRT}{P_L^2} + \beta V_f\right). \tag{3}$$

The volume change at the diaphragm (∂V_d) is the summation of volume displaced by the syringe (∂V_s) and hydraulic line compression (∂V_L) (Eq. (4)),

$$\partial V_d = \partial V_s + \partial V_L. \tag{4}$$

Next, we define diaphragm stiffness (k_d, [N/m^5]) as the parameter relating change in pressure across the diaphragm ($\partial P_L - \partial P_o$, [Pa]) to change in displaced volume (∂V_d), which, in general, is a function of the pressure difference across the diaphragm ($P_L - P_o$, [Pa]), which need not be linear (Eq. (5)),

$$\frac{\partial P_L - \partial P_o}{\partial V_d} = k_d = f(P_L - P_o). \tag{5}$$

Notice that ∂V_d is equal to the volumetric displacement of the deposition liquid. If the deposition liquid is incompressible and completely fills the reservoir cavity with no entrapped air, ∂V_d is equal to the liquid volume displaced through the capillary tip (∂V_o, [m^3]). We assume this is true for the present case.

We define the sensitivity (S) of the dispenser as the ratio of volumetric displacement of the diaphragm (∂V_d) to the volumetric displacement of a syringe stroke (∂V_s). By algebraic substitution of Eqs. (1)–(5), we derived an expression for dispenser sensitivity as a function of two dimensionless parameters, C and D (Eq. (6)),

$$S = \frac{\partial V_d}{\partial V_s} = \frac{1}{1+C} - \frac{DC}{(1+C-D)(1+C)} = S_H - S_D, \tag{6a}$$

$$C = k_d\left(\frac{nRT}{P_L^2} + \beta V_f\right) \approx \frac{k_d nRT}{P_L^2}, \tag{6b}$$

$$D = \frac{\partial P_o}{\partial P_L}. \tag{6c}$$

First, the compressibility parameter, C (Eq. (6b)), relates all system parameters affecting hydraulic line compressibility. All physically significant parameter values (n, R, T, P_L, k_d, β, V_f), and thus C, are lower-bounded at zero. For C to be greater than zero, it is necessary to have entrapped air (n) and/or fluid compressibility (β). Notably, C may be adjusted by varying the line pressure (P_L). Unlike k_d and n, which are fixed by the system design and assembly, P_L can be easily varied by syringe actuation. Hydraulic fluid compressibility is negligible because we use water ($\beta = 46 \times 10^{-11}$ Pa^{-1} at 25 °C) and maintain $P_L < 200$ kPa due to the limit of our pressure transducer.

Second, the disturbance parameter, D (Eq. (6c)), is the ratio of the pressure change on the downstream (deposition liquid) side of the diaphragm (∂P_o) to the change in line pressure (∂P_L). The pressure exerted on the diaphragm during deposition of liquid onto a substrate constitutes ∂P_o; for example, a disturbance can be introduced by the capillary pressure arising from tip-liquid-substrate interactions. $D = [0,1]$ for physically significant states of the system. When $D = 0$, the deposition fluid experiences no change in pressure upon actuation of the diaphragm (i.e., $\partial P_o = 0$). Physically, this means that the deposition fluid imparts no resistance on being volumetrically displaced by the diaphragm. For $D = 1$, the deposition fluid experiences a change in pressure exactly equal to that in the hydraulic line upon syringe actuation. Equation (5) shows that this results in zero diaphragm deformation (i.e., $\partial V_d = 0$). Physically, this corresponds to the situation in which the deposition fluid is incompressible and plugged such that it cannot undergo volumetric displacement. The system may approach this condition, if, for example, capillary pressure at the end of the deposition tip becomes large. This may be true if very small diameter tips are used.

We have formulated the equation for dispenser sensitivity (Eq. (6a)) to highlight two terms. It is composed of a hydraulic sensitivity term (S_H) which is solely dependent on C. Subtracted from S_H is a disturbance sensitivity term (S_D) that depends on both C and D. Because C is always greater than zero, S_H is bounded between 0 and 1. For the limiting case where the hydraulic line approaches perfect incompressibility ($C \to 0$), dispenser sensitivity approaches 1 regardless of the pressure disturbances (i.e., $S_H = 1$, $S_D = 0$). This is also depicted in Fig. 3(c). Conversely, as line compressibility becomes very large ($C \to \infty$), dispenser sensitivity approaches zero regardless of the pressure disturbances (i.e., $S_H = 0$, $S_D = 0$). For zero pressure disturbance ($D = 0$), dispenser sensitivity is simply described by S_H since S_D equals zero. As D increases, the nonlinear curve describing the relation between S and C shifts left (Fig. 3(c)), which lowers the dispenser sensitivity for a prescribed value of C. Finally, at maximum disturbance ($D = 1$), dispenser sensitivity is zero because S_H equals S_D, and may be regarded, visually, as an infinite leftward shift of the S–C curve.

To measure the hydraulic line compression, we plugged fluid line 1 with a solid-state pressure transducer just upstream of the diaphragm (Fig. 4(a)). In this configuration, we actuated the syringe (ΔV_s, [m^3]) and recorded P_L, noting that ΔV_s must be equal to the volume change of the hydraulic line (ΔV_L, [m^3]). We found the relationship between line pressure and syringe displacement to be inversely proportional (Fig. 4(b)) and the transmission of pressure from syringe to sensor to be essentially instantaneous (Fig. 4(c)). This confirms that hydraulic line compression is due to entrapped air, and is accurately described by the ideal gas law.

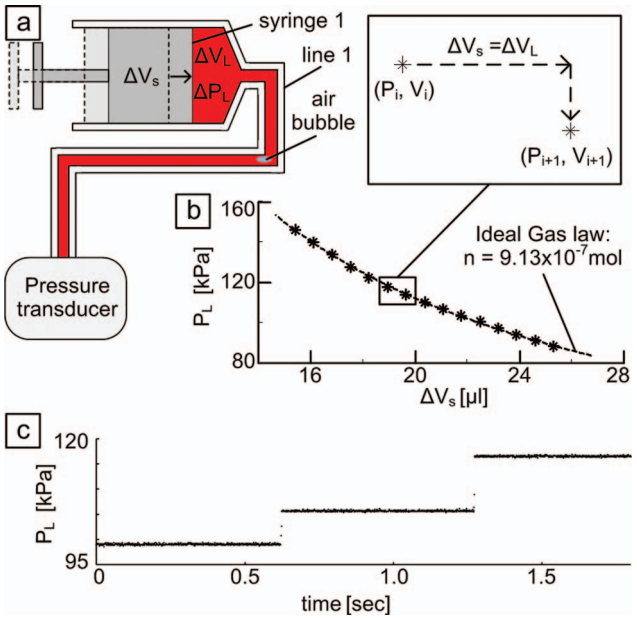

FIG. 4. (Color online) Validation of fluid line compressibility due to entrapped air: (a) plugged configuration of the hydraulic line used for these measurements; (b) inverse relation between line pressure and volumetric displacement, which is described by the ideal gas law; (c) pressure transients in the line upon syringe actuation, verifying that pressure transmission is essentially instantaneous.

We derived an expression, based on the ideal gas law, to calculate the amount of entrapped air (n) using line pressure measurements before (P_i) and after (P_{i+1}) a syringe stroke of known volumetric change (ΔV_s) (Eq. (7)),

$$n = \frac{P_i P_{i+1} \Delta V_s}{RT\,(P_i - P_{i+1})}. \tag{7}$$

Here, $\Delta V_s > 0$ corresponds to an increase in hydraulic line volume, and thus a decrease in pressure. We performed this calculation between sequential points in Fig. 4(b), and determined $n \approx 0.9$ μmol.

We then measured the sensitivity of the dispenser experimentally, having the system assembled as shown in Fig. 3(a). We filled the reservoir cavity and capillary with water through the inlet, as described in Sec. II A. Then, we plugged the inlet and actuated the diaphragm forward until a small liquid bulge extended from the tip (Fig. 3(b)). From here, we actuated the syringe by a small stroke and recorded the volume change of the liquid bulge, noting that $\Delta V_d = \Delta V_o$ in this case. This volume change was determined by image analysis, assuming that the bulge geometry is a spherical cap. We assumed that this incremental volume change was small enough so that $\Delta V_d/\Delta V_s \approx \partial V_d/\partial V_s = S$. We repeated this procedure at a range of line pressures, showing that S increases as P_L increases, and ranges from 2.7×10^{-3} to 9.9×10^{-3} (Fig. 3(e), circles). We performed the measurements

so as to keep ΔV_o approximately the same for all data points.

Based on these measurements, we approximated the effect of capillary pressure against the diaphragm (P_o) using the Laplace-Young equation for capillary pressure across a spherical curved meniscus (Eq. (8)). P_{atm} is the ambient pressure, P_{head} is the head pressure from the water column inside the capillary tube, γ is the water-air surface tension at room temperature ($\gamma = 0.0728$ N/m), and r is the meniscus radius of curvature,

$$P_o = \frac{2\gamma}{r} + (P_{\text{atm}} - P_{\text{head}}). \tag{8}$$

The change in capillary pressure (ΔP_o) was computed using measurements of the liquid bulge radius of curvature before (r_1) and after (r_2) each ΔV_s (Eq. (9)),

$$\Delta P_o = 2\gamma \left(\frac{1}{r_2} - \frac{1}{r_1}\right). \tag{9}$$

We then substituted Eq. (9) into Eq. (6a) by assuming that $\Delta P_o \approx \partial P_o$ (Eq. (10)), and found k_d to be approximately constant across all measurements ($k_d \approx 9 \times 10^{14}$ N/m^5),

$$k_d = \frac{P_L^2 r_1 r_2 (\Delta V_s - \Delta V_d) + 2nRT\gamma (r_2 - r_1)}{\Delta V_d nRT r_1 r_2}. \tag{10}$$

Using the experimental sensitivity measurements, and the calculated values for n and k_d, we calculated the corresponding non-dimensional terms C and D using Eq. (6). Our maximum and minimum measurable line pressures ($P_{\text{Lmax}} = 124$ kPa, $P_{\text{Lmin}} = 70$ kPa) correspond to C ranging from 95 to 350, respectively. D is approximately constant ($D \approx 0.05$) for all measurements, which is expected since ΔV_o was approximately the same for all measurements. We show that the experimental S measurements (Figs. 3(c)–3(e), circles) fit well against model curves plotted using our calculated values for n, k_d, and D (Figs. 3(d) and 3(e), dotted lines).

This model guides us on how to configure the system to achieve a desired resolution, and enables understanding of how capillary pressure at the tip affects the dispenser performance. Our sensitivity measurements show that the dispenser currently exhibits approximately 100:1 to 370:1 deamplification of the syringe's volumetric displacement at the diaphragm. Considering that the displacement resolution (ΔV_s) of our custom syringe pump is < 2.0 nl, these sensitivity values indicate that we can control the displacement of liquid at the capillary tip (ΔV_o) with resolutions ranging from ~5 to 20 pl.

A notable characteristic of this system is that, for a given line compressibility C, disturbances due to capillary pressure (i.e., $D > 0$) serve to lower system sensitivity. Capillary pressure disturbances will become more significant at smaller size regimes due to larger meniscus curvatures. Therefore, we expect the resolution of the system to inherently scale with droplet volume since D will become more significant. If the sensitivity measurements described above were conducted using a capillary tip inner diameter smaller by one order of magnitude (45 μm), we estimate $S \sim 6 \times 10^{-6}$ and $D \approx 0.998$ by extrapolation of our model. This indicates that our current system will exhibit volumetric resolution on the order of

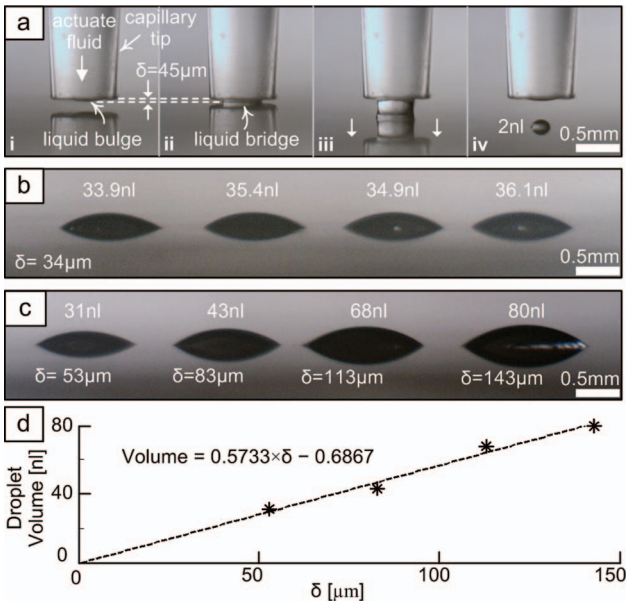

FIG. 5. (Color online) Contact printing of droplets using liquid bridges: (a) still images showing steps in the procedure, resulting in deposition of a droplet with 2 nl volume (enhanced online) [URL: http://dx.doi.org/10.1063/1.3673680.1]; (b) row of four droplets with identical volumes, deposited sequentially; (c) row of four droplets with different volumes, deposited sequentially; (d) relationship between droplet volume and liquid bridge height (δ).

0.1 pl without any modification. In this respect, inclusion of an air bubble in the hydraulic line is advantageous because a perfectly incompressible hydraulic line would not scale the resolution with the droplet size.

We emphasize that our model describes the volumetric control of a pinned volume of liquid at stable equilibrium capillary pressure conditions. Examples include a liquid bulge extending from the end of a capillary tip, as utilized for the sensitivity measurements, and a liquid bridge spanning between the capillary tip and a substrate (Fig. 5(a)). In other words, our model describes the precision with which the volume of a stable liquid bridge or bulge may be increased or decreased once established. Instabilities, such as stick-slip of liquid contact lines, and liquid bridge collapse, can drastically alter the equilibrium capillary pressure condition within a liquid volume and are often difficult to predict. These events may cause sudden, microliter, displacements of liquid through the capillary tip. This is not captured by our consideration of Laplace capillary pressure disturbances for describing system sensitivity. In principle, analytical models for dynamic scenarios involving instabilities could be derived, but this is beyond the scope of the present study. Such a model would relate the particular instability to the pressure exerted on the diaphragm (∂P_o), which could then be substituted into Eq. (6).

Additionally, resolution of the dispenser can be improved by increasing k_d or n. These parameters can be modified by replacing the diaphragm, and injecting air into the hydraulic line. Although Eq. (6) suggests that infinitesimal volumetric resolution can be achieved using a sufficiently large entrapped air bubble and a very stiff diaphragm, there are, of course, practical limitations including room

vibrations, temperature fluctuations, and syringe volume capacity.

IV. RESULTS

We now demonstrate the functionality of the dispenser to controllably deposit liquid droplets on substrates, and to manipulate a liquid meniscus between the capillary tip and substrate. We then demonstrate the effect of droplet size and temperature on the evaporative assembly of microspheres, and use capillary tip rotation to control the 3D organization of microrods. These results are enabled by simultaneous control of liquid displacement using the diaphragm pump, stage motion, and optional capillary tip rotation.

A. Direct-write droplet deposition by liquid bridging

The bidirectional pumping capability allows discrete liquid droplets to be deposited from the capillary tip by contact printing. After the reservoir is loaded, as described in Sec. II A, we actuate the diaphragm forward, by manual control of the syringe pump, to cause the deposition liquid to bulge outward from the capillary tip (Fig. 5(a), enhanced online). We monitor the size of the bulge using a video microscope with dashed-line markers overlaid on-screen to denote the distance, δ, from the edge of the capillary tip to the apex of the liquid bulge. Then, we move the substrate upward until it contacts the bulge at distance δ from the capillary tip, causing a liquid bridge to form. Then, we lower the substrate using the motorized stage, causing the bridge to neck and break, printing a droplet on the substrate.

We consider the distance δ to be a metric relating the volume of the initial liquid bulge to the volume of the printed droplet. Larger δ corresponds to a larger bulge volume, and therefore, a larger printed droplet. To control the droplet volume, we incrementally actuate the syringe pump while referencing the video feed. We set the liquid bulge to the desired δ before each deposition. The droplet volume can then be calculated from the video microscope images, by measuring the droplet height and contact line diameter, and assuming a spherical cap geometry.

Figure 5 shows three limiting examples of this technique. First, (Fig. 5(a), iv) shows a water droplet as small as 2 nl ($\delta = 45$ μm), deposited using a capillary tip with 450 μm inner diameter onto a plastic microscope coverslip substrate. Next, we deposited multiple mineral oil droplets at the same δ, which shows that the contact printing procedure is repeatable (Fig. 5(b)). The low vapor pressure of mineral oil minimized evaporation, which allowed us to sequentially deposit the four 35 nl (standard deviation of 0.9 nl) droplets and then take the image shown to measure the droplet volumes. We also deposited mineral oil droplets at different values of δ (Fig. 5(c)), and show that the relation to droplet volume is approximately linear within the range tested (Fig. 5(d)). Several other parameters affect the printed droplet volume, including the capillary tip material and geometry, and the air/liquid/substrate surface energies. In general, performance of the machine will depend on these parameters, which can be calibrated in advance. In the future, we imagine implementing closed-loop positional control for the 3D stage and syringe pump stepper motor to improve position and volume displacement accuracy beyond the manual proof-of-concept shown here.

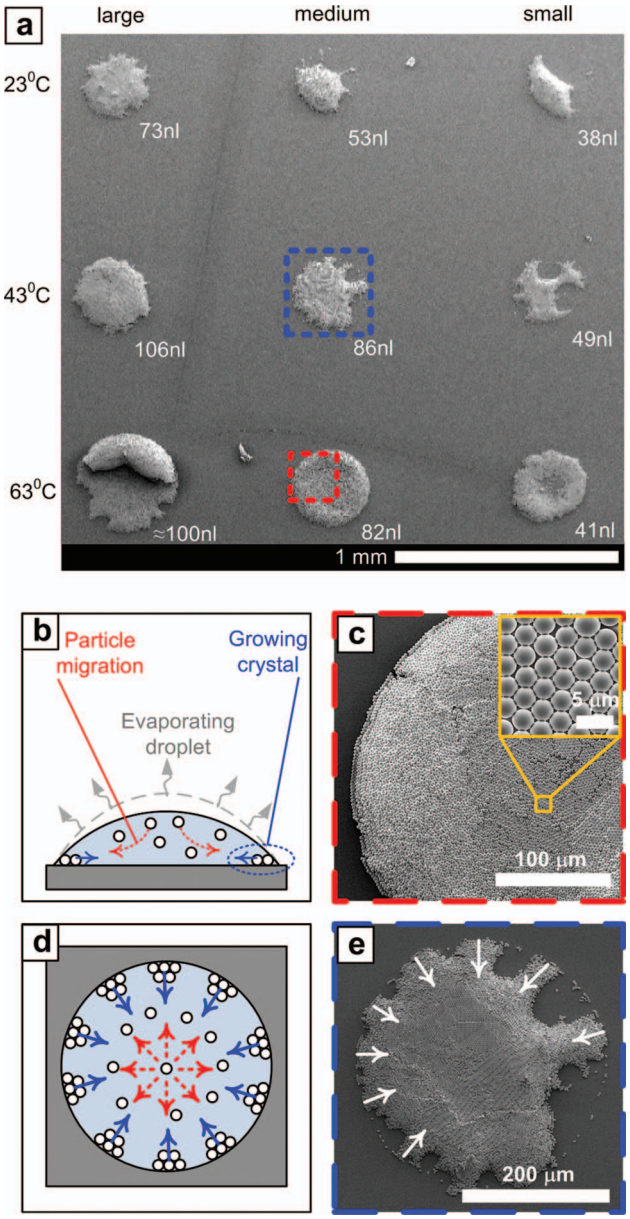

FIG. 6. (Color online) Assembly of polystyrene microspheres from droplets deposited by contact printing: (a) Three-by-three array of self-assembled particle crystal islands formed from droplets with different volumes deposited at different temperatures; (b) schematic of self-assembly process in the drying droplets; (c) SEM of uniform crystal island at optimum temperature and droplet volume (inset: closely-packed assembly of 3 μm polystyrene spheres in this island); (d) schematic of heterogeneous nucleation and growth of particle crystals at the contact line; (e) SEM of a non-uniform crystal island having the finger-like protrusions.

B. Evaporative self-assembly of microspheres and microrods

Using our contact-printing technique, we deposited a 3 $\times$ 3 array of droplets consisting of a water-based suspension containing 3 μm-diameter polystyrene particles (2.5 vol. %, Polysciences, Inc.). Temperature was varied by row and droplet volume by column (Fig. 6(a)). Thus, this is a small

combinatorial study of the evaporation-induced self-assembly of micro-particles. A uniform polycrystalline island with diameter ≈ 350 μm is achieved at $T = 63$ °C and $V = 82$ nl (Fig. 6(c)).

We consider two major effects when interpreting these results. First, the diameter of the assembled microparticle crystal correlates with the diameter of the initial liquid-substrate contact area. This diameter is dependent on the droplet volume and contact angle. Because substrate temperature affects the contact angle, it affects the droplet volume and wetting diameter. Second, in the absence of evaporation, the particle concentration of the source solution (inside the capillary tip) should match the particle concentration inside a deposited droplet. Accordingly, the number of particles in each deposited droplet would scale linearly with the droplet volume. However, elevated substrate temperature significantly increases the evaporation rate so that the particle concentration continuously increases during the bridging stage of droplet deposition. In this respect, the particle concentration in deposited droplets is directly related to the substrate temperature, and this may be exploited to control the volumetric concentration of particles in deposited droplets. We observe these effects in the array because the number of particles per island increases with volume and with temperature.

During evaporation of these deposited droplets, the particle concentration increases and particles migrate towards the liquid-substrate contact line,[22] as depicted in Fig. 6(b). Here, particle crystals nucleate and grow towards the center of the droplet (Fig. 6(d)) until evaporation completes. If the droplet does not contain a sufficient number of particles, crystal growth from the nucleation cites may cease due to starvation of particles. In such a case, there are several finger-like structures protruding inward from the location of the pinned contact line, as shown in Fig. 6(e).

Finally, we demonstrate the effect of capillary tip rotation on the assembly of polymer micro cylinders[23] from a water-based solution. At constant rotation rate (12 rpm) and elevated substrate temperature (60 °C), we established a liquid bridge between the capillary tip and substrate (Fig. 7(a)). Then, we moved the substrate downward slowly while dispensing. This continuous stretching and twisting of the meniscus assembled the micro cylinders into a 3D chiral structure (Fig. 7(b), enhanced online). By tuning the rotation speed, downward motion speed, and substrate temperature, 3D structures having different geometries may be achieved.

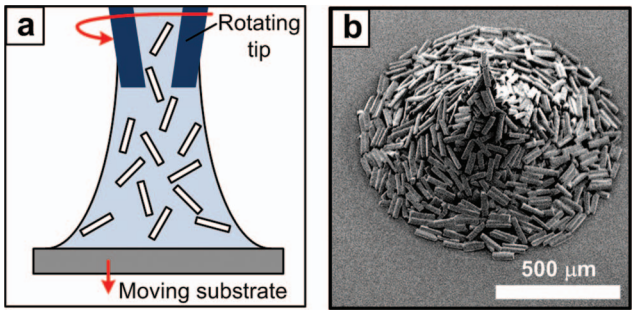

FIG. 7. (Color online) Simultaneous dispensing and assembly of micro-rods into a 3D chiral assembly using the rotating capillary tip: (a) schematic of the process; (b) SEM image of a chiral assembly fabricated by this process (enhanced online). [URL: http://dx.doi.org/10.1063/1.3673680.2].

V. CONCLUSION

We designed, built, and tested a rate-controlled sub-nanoliter resolution dispenser system, and demonstrated its utility for direct-write droplet deposition and evaporative self-assembly. The system features four degrees of freedom between a deposition tip and a temperature-controlled substrate. Simultaneous actuation of the liquid dispenser along with motion of the stage enables spatial and temporal control of the meniscus profile of evaporating droplets. We expect the resolution of the system to inherently scale with the droplet volume, allowing us to deposit and manipulate picoliter or smaller liquid volumes with properly designed deposition tips. We envision this machine being an essential tool for proof-of-concept demonstration of unique 2D and 3D particle assemblies, and a versatile platform for studying the principles of capillary self-assembly across the micro- and nanoscales.

ACKNOWLEDGMENTS

This project began in the Mechanical Engineering 450 senior design course at the University of Michigan. We thank Lawrence Petigrow for his contributions as a team member of the ME450 project; Professor Samantha Daly for use of a micromechanical tester in her laboratory; and Jaewon Yoon and Professor Joerg Lahann for providing polymer microcylinders. Financial support was provided by the Department of Energy Office of Basic Sciences (DE-SC0004927) for system assembly, testing, and preparation of the manuscript; and the University of Michigan via startup funds to A.J.H. for procurement of the system components and sponsorship of the ME450 project. J.B. acknowledges a National Science Foundation Graduate Research Fellowship. Electron microscopy was performed at the University of Michigan Electron Microbeam Analysis Library (EMAL).

[1] D. V. Talapin, J. S. Lee, M. V. Kovalenko, and E. V. Shevchenko, Chem. Rev. **110**(1), 389 (2010).
[2] S.-H. Kim, S. Y. Lee, S.-M. Yang, and G.-R. Yi, NPG Asia Mater. **3**(1), 25 (2011).
[3] S. K. Ghosh and T. Pal, Chem. Rev. **107**(11), 4797 (2007).
[4] A. Zabet-Khosousi and A. A. Dhirani, Chem. Rev. **108**(10), 4072 (2008).
[5] C. L. Haynes, A. D. McFarland, M. T. Smith, J. C. Hulteen, and R. P. Van Duyne, J. Phys. Chem. B **106**(8), 1898 (2002).
[6] J. F. Li, Y. F. Huang, Y. Ding, Z. L. Yang, S. B. Li, X. S. Zhou, F. R. Fan, W. Zhang, Z. Y. Zhou, D. Y. Wu, B. Ren, Z. L. Wang, and Z. Q. Tian, Nature (London) **464**(7287), 392 (2010).
[7] N. D. Denkov, O. D. Velev, P. A. Kralchevsky, I. B. Ivanov, H. Yoshimura, and K. Nagayama, Langmuir **8**(12), 3183 (1992).
[8] K. Nagayama, Colloids Surf., A **109**, 363 (1996).
[9] L. F. Chen and J. R. G. Evans, Langmuir **25**(19), 11299 (2009).
[10] S. Choi, S. Stassi, A. P. Pisano, and T. I. Zohdi, Langmuir **26**(14), 11690 (2010); M. Rycenga, P. H. C. Camargo, and Y. N. Xia, Soft Matter **5**(6), 1129 (2009).
[11] E. Kim, Y. N. Xia, and G. M. Whitesides, Adv. Mater. **8**(3), 245 (1996).
[12] S. McGuire, C. Fisher, M. Holl, and D. Meldrum, Rev. Sci. Instrum. **79**(8), 3 (2008).
[13] K. Wang and J. P. W. Stark, Appl. Phys. A **99**(4), 763 (2010).

[14]P. Ferraro, S. Coppola, S. Grilli, M. Paturzo, and V. Vespini, Nat. Nanotechnol. **5**(6), 429 (2010).
[15]I. Barbulovic-Nad, M. Lucente, Y. Sun, M. J. Zhang, A. R. Wheeler, and M. Bussmann, Crit. Rev. Biotechnol. **26**(4), 237 (2006).
[16]L. Chen, Y. Zhang, S. Yang, and J. R. G. Evans, Rev. Sci. Instrum. **78**, 072210 (2007).
[17]B. J. Larson, S. D. Gillmor, and M. G. Lagally, Rev. Sci. Instrum. **75**(4), 832 (2004).
[18]G. M. Gratson, M. J. Xu, and J. A. Lewis, Nature (London) **428**(6981), 386 (2004); B. Y. Ahn, D. Shoji, C. J. Hansen, E. Hong, D. C. Dunand, and J. A. Lewis, Adv. Mater. **22**(20), 2251 (2010).
[19]B. Y. Ahn, D. J. Lorang, E. B. Duoss, and J. A. Lewis, Chem. Commun. **46**(38), 7118 (2010).
[20]N. C. Schirmer, S. Strohle, M. K. Tiwari, and D. Poulikakos, Adv. Funct. Mater. **21**(2), 388 (2011).
[21]L. van Laake, A. J. Hart, and A. H. Slocum, Rev. Sci. Instrum. **78**(8), 9 (2007).
[22]R. D. Deegan, O. Bakajin, T. F. Dupont, G. Huber, S. R. Nagel, and T. A. Witten, Nature (London) **389**(6653), 827 (1997).
[23]S. Bhaskar, J. Hitt, S. W. L. Chang, and J. Lahann, Angew. Chem., Int. Ed. **48**(25), 4589 (2009).